Engineering Failure Analysis 160 (2024) 108172

Contents lists available at ScienceDirect

Engineering Failure Analysis

journal homepage: www.elsevier.com/locate/engfailanal

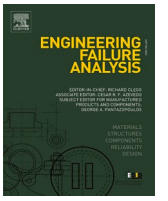

Mode-I fracture toughness of hygrothermally aged curved filament-wound carbon and glass fibre composites

Artur Pollet [a,d], José Humberto S Almeida Jr [b,*], Antonios G Stamopoulos [c], Sandro C. Amico [a]

[a] PPGE3M/PROMEC, Federal University of Rio Grande do Sul, Porto Alegre, RS, Brazil
[b] School of Mechanical and Aerospace Engineering, Queen's University Belfast, Belfast, UK
[c] Department of Industrial and Information Engineering and Economics (DIIIE), University of L'Aquila, Montelucco di Roio, L'Aquila, Italy
[d] SENAI Institute of Innovation in Polymer Engineering, São Leopoldo, RS, Brazil

ARTICLE INFO

Keywords:
Fracture toughness
Hygrothermal ageing
Curved structures
Filament winding

ABSTRACT

This work aims to assess the effect of hygrothermal ageing on the Mode-I fracture toughness behaviour of glass/epoxy and carbon/epoxy composites manufactured by filament winding. Cylinders (136 mm in diameter) are manufactured using various winding angles (±0°, ±15°, ±30° and ± 45°), and the specimens are aged in water at room temperature and 70 °C. Water uptake was monitored until equilibrium, which varies with the material, temperature, and winding angle, being the highest for the ± 45° sample, reaching 1.10 % for glass/epoxy and 1.74 % for carbon/epoxy at room temperature, and 1.30 % and 2.95 % at 70 °C. These results are related to the void content, which is 3.20 % and 3.41 %, respectively. Glass/epoxy composites show superior performance in terms of peak load and strain energy release rate, but carbon/epoxy shows higher fracture toughness for the same winding angle and ageing. Specimens aged at room temperature are less prone to delamination than those at 70 °C. In addition, aged samples at room temperature show higher peak force and strain energy release rates compared to non-aged composites, which is attributed to matrix plasticisation. Samples aged in hot water have poorer behaviour compared to those non-aged or aged at room temperature. The curved double cantilever beam (CDCB) samples have more complex fracture mechanisms compared to flat samples, attributed to their curvature and difficulty in keeping symmetry throughout the test.

1. Introduction

Filament winding is a widely used technique for producing composite pressure vessels for gas storage and transportation [1]. The introduction of composite materials as the primary material in the gas storage sector has enabled the transition from Type I pressure vessels, typically used in compressed natural gas (CNG) storage applications, to Type IV, more suitable for hydrogen [2]. As a manufacturing process, it consists of depositing reinforcing tows onto a rotating mandrel (or liner), creating interlaced layers of composites [3,4], and providing a certain level of automation and adaptability to manufacturing parameters.

Since failure of filament-wound composite structures is critical for safety/reliability reasons, many studies were published on investigating the effect of process parameters on the development of defects as well as on the performance of tubes or pressure vessels

* Corresponding author.
E-mail address: Humberto.almeida@qub.ac.uk (J.H.S. Almeida Jr).

https://doi.org/10.1016/j.engfailanal.2024.108172
Received 24 October 2023; Received in revised form 2 January 2024; Accepted 24 February 2024
Available online 28 February 2024

[3,5,6]. These works mostly focus on the identification of manufacturing defects, the development of accurate numerical tools for predicting the effect of fabrication on performance, or the experimental assessment of the performance of these structures. Related to the former, non-invasive evaluation methods for detecting phenomena such as fibre undulation [5], voids [3,6] or deviation of the winding angle from the desired value [3] can be found. As for the development of numerical models, the effect of cylinders loaded under axial compression, torsion and internal pressure was numerically assessed by de Menezes et al. [7], who predicted the effect of local stress concentration on the overall performance of composite cylinders considering the winding pattern formed during the winding process [8]. Chang et al. [9] numerically evaluated the effect of the winding pattern on the strength of multi-axially loaded filament-wound cylinders, and Uddin et al. [10] performed simulations to evaluate the strength of filament-wound flywheel disks.

A critical aspect of the simulation is the accurate validation of models based on case-specific mechanical tests, or the assessment of mechanical or structural characteristics of filament-wound structures. Indeed, an increasing number of works are dedicated to the experimental characterisation of these structures, such as axial compression of hollow cylinders [11] or both radial compressive and tensile tests using rings cut from filament-wound tubes [12].

A particularly interesting testing category is to assess interlayer fracture toughness. In the case of filament-wound structures, the curved double-cantilever beam (CDCB) geometry has been reported in a growing yet small number of works. The use of curved specimens may introduce mixed mode stresses on the crack tip when coupled with asymmetric configurations. Therefore, the initiation and propagation of cracks may vary compared to flat structures.

The CDCB sample was introduced by Foral [13] and applied to thermoplastic filament-wound structures by Lauke and Friedrich [14] who further discussed its effectiveness. More recently, Ozdil et al. [15] characterised interlaminar crack growth in a curved sample extracted in the longitudinal direction from a $[\pm 30]_{12}$ glass/epoxy filament-wound cylinder. Whereas Perillo and Echtermeyer [16,17] reported more reliable measurements of Mode-I fracture toughness for glass fibre/epoxy filament-wound structures using transversally extracted curved samples. Furthermore, Rased and Yoon [18] and Taylor et al. [19] reported that the curvature of the samples is acceptable if the specimens mimicked the lay-up of the equivalent filament-wound structure.

Another noteworthy aspect of these structures concerns the effect of in-service environmental conditions. More precisely, the combination of humidity and thermal cycles may cause the so-called hygrothermal ageing of the structure. Indeed, moisture absorption combined with thermal cycles may severely damage the composite structure. In the work of Ray [20], the moisture uptake in carbon and glass/epoxy fibre composites has been found to lead to fibre damage and matrix degradation. Taking this into consideration, Krishnan et al. [21] studied the effect of hygrothermal ageing on the multi-axial load-bearing capacity of $[\pm 55]_4$ glass/epoxy wound cylinders and showed that fibre/matrix debonding may cause premature failure. Similar observations were reported by Itriah et al. [22] who found a decrease in axial compressive strength of glass fibre/epoxy wound tubes. Also, the decrease in burst strength after the impact of hygrothermally aged $[\pm 55]_6$ glass/epoxy tubes was presented by Hawa et al. [23]. Nevertheless, the hygrothermal effect on the interlayer fracture behaviour of filament-wound structures is yet to be studied.

In this work, the effect of the hygrothermal ageing on the Mode-I fracture toughness of both glass and carbon fibre/epoxy filament-wound composites is studied using curved DCB (CDCB) specimens and following established testing standards, for winding strategies ranging from hoop ($\pm 90°$) to helicoidal ($\pm 45°$). In addition, the combined moisture-temperature effect on the toughness of the curved structures was investigated using water at room temperature and 70 °C.

2. Experimental details

2.1. Materials

The composite cylinders are manufactured using either towpregs of carbon fibre (T700SC-12 K-50C) or glass fibre (158B-AB-450), both from Toray (Tokyo, Japan). The epoxy resin is the UF3369-100 for both towpreg systems, from TCR Composites (Ogden, USA). The fibre volume fraction is ≈60 % in both systems.

A cylindrical stainless-steel mandrel (diameter: 136 mm; length: 300 mm) was used. A liquid epoxy mould release agent Loctite® Frekote 770-NC was applied to the mandrel to assist in the cylinder removal. A PTFE tape (63 mm wide, 13 μm thick) from Anay has been used to introduce the pre-crack. In a typical DCB test, the load may be applied throughout a pair of load blocks or piano hinges [20–26]. In this work, the ending/load blocks were chosen since they can be more easily implemented in the curved sample. These blocks are made of AISI 1020 and one of the surfaces is machined to match the curvature of the mandrel. An epoxy-based structural adhesive (HAI) was used to bond the specimen to the blocks.

2.2. Manufacturing

The cylinders are manufactured via a dry filament winding process. The design and winding path of the cylinders are made using the CADWIND software [27] model V10. The bandwidth of the carbon/epoxy and glass/epoxy towpregs are 2.3 and 2.1 mm, respectively. Despite the different bandwidths, both laminates are manufactured with a similar degree of coverage (c.a. 100 %). A KUKA robot with 7 degrees of freedom and an angle tolerance of 0.1° with peripherical devices from MFTECH has been used to wind the towpregs onto the abovementioned mandrel.

One family of samples was made using a hoop trajectory ($\pm 90°$), and three other families with non-geodesic helicoidal trajectories at angles of $\pm 75°$, $\pm 60°$ and $\pm 45°$, with a winding pattern of 1/1. The process parameters are carefully selected to obtain comparable samples, so that fibre angle is the only noticeable variable. It is worth mentioning that the axial direction of the cylinder is offset by 90° in comparison to the sample mounted in the DCB rig. Therefore, the fibre angle in the cylinders wound at $\pm 90°$, $\pm 75°$, $\pm 60°$ and $\pm 45°$

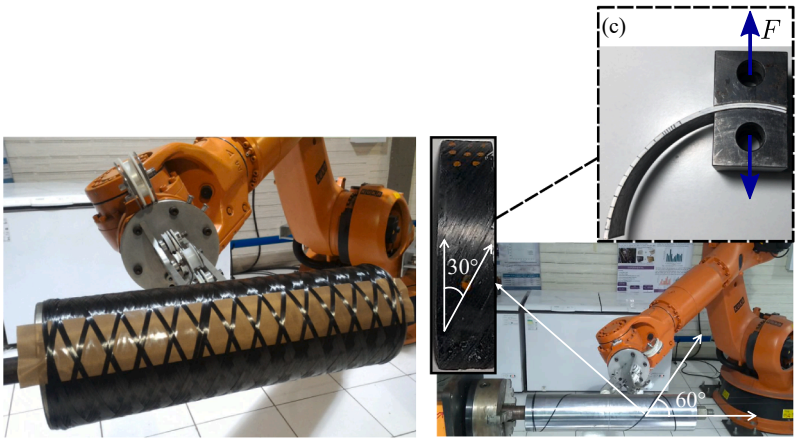

Fig. 1. (a) Use of the PTFE film during winding, (b) fibre angle illustration, and (c) specimen glued to the ending blocks for the CDCB test.

are hereafter referred to as ± 0°, ±15°, ±30° and ± 45°, respectively. This way, the transverse-like CDCB specimen could a be reasonably pure Mode-I crack opening [27]. Fig. 1**(a)** shows the insertion of the PTFE film during the manufacturing at the neutral axis of the laminate, while Fig. 1**(b)** illustrates the angle difference comparing manufacturing and testing.

After winding, the sample/mandrel system is placed in an oven for 4 h at 120 °C for curing, and the cylinder is later extracted from the mandrel. A diamond saw is used to cut the specimens for testing (width: 25 mm, length: 125 mm). Some samples are analysed in a Carl Zeiss optical microscope to quantify void, fibre, and resin volume fractions, assuming that these samples are representative of the structure.

2.3. Hygrothermal ageing

Hygrothermal ageing is carried out on some samples prior to the CDCB tests. For that, the edges of the samples are sealed with polyester resin to prevent water uptake through the thickness. Then, the samples are immersed in a water bath at room temperature (23 °C) or at 70 °C for 66 days. Eight samples of each family are used, totalling 64 for each material system.

The entire procedure follows the recommendations of the ASTM D5229-20 standard. The mass of the samples is measured periodically, and water absorption is calculated as:

$$M(\%) = \frac{(M_w - M_d)}{M_d} \times 100 \tag{1}$$

where M_w and M_d are the wet and dry masses, respectively.

The diffusion mechanism and moisture absorption are studied based on Fick's law [28,29], as follows:

$$M = M_\infty \left[1 - exp\left(-7.3 \left(\frac{Dt}{h^2} \right)^{\{0.75} \right\} \right) \tag{2}$$

where M is water uptake at a particular time t, M_∞ is the mass at a quasi-equilibrium state, D is the diffusion coefficient, and h is the sample thickness. The diffusion coefficient D is calculated from the absorption curve, as follows:

$$D = \pi \left(\frac{h}{4M_\infty} \right)^2 \left(\frac{M_2 - M_1}{t_2^{\frac{1}{2}} - t_1^{\frac{1}{2}}} \right)^2 \tag{3}$$

2.4. CDCB tests

The CDCB tests are carried out following the recommendations of the ASTM D5528/5528 M−21 standard. Although this standard focuses on flat samples, this is the closest standard available as a guide to these tests. The lateral surfaces of the samples are painted white to monitor crack growth, and the ending blocks (radius of 68 mm) are attached to the sample with the adhesive. The ending blocks + specimen system (Fig. 2) is then attached to an Instron (model 3382) Universal Testing Machine with a 100 N load cell.

Fig. 2. Illustration of the testing rig.

The CDCB test (Fig. 2) is performed in two steps. Firstly, the pre-crack grows up to 2–5 mm to remove eventual resin pockets or other defects that arise from the PTFE tape insertion at the crack front, for more reliable results. The system is then fully unloaded until zero displacement with a constant crosshead displacement of 8 mm/min. After that, the actual test takes place with a crosshead speed of 1 mm/min, which corresponds to the lowest suggested by the referred standard. The crack tip is monitored with a digital microscope (maximum zoom of 1600 ×) for correlating applied load, crosshead displacement and crack extension. The definition of the crack initiation point is conducted using the VIS point technique. In general, such a load–displacement curve is composed of a quasi-linear part that corresponds to the crack initiation when the load reaches the peak value and a crack propagation region after that. The load smoothly decreases in the case of stable crack propagation. Nevertheless, a potentially unstable crack propagation may cause a sudden load drop. As mentioned, the crack extension is monitored visually and correlated to the load applied by the testing machine and the related displacement at every 5 mm of crack extension.

Once the test is concluded, the strain energy release rate (G_1) is calculated through the modified beam theory:

$$G_1 = \frac{3P\delta}{2b(a + |\Delta|)} \tag{4}$$

where P is the force, δ is the displacement, b is the width of the sample, a is the crack length, and $|\Delta|$ is calculated through the interception point between the compliance $C^{\frac{1}{3}}$ – crack length a curve and the axis of the crack length. The compliance is defined as:

$$C = \frac{\delta}{P} \tag{5}$$

3. Results

3.1. Hygrothermal ageing and void analyses

The water uptake of the composite structures is closely related to the voids, which can be seen as resin air pockets. In Fig. 3, the mean and standard deviation values of void content for all specimens are presented. The lowest void content was found for the hoop wound samples and the highest for the ± 45° winding angle, perhaps due to the lower tow tensioning during winding. Besides, the standard deviation generally increases from ± 0° to ± 45°, especially for glass/epoxy, indicating more heterogeneous samples.

In Fig. 4, a comparison between experimental values of water absorption for both glass and carbon/epoxy composites and the Fick's law prediction is presented. The agreement is very good, especially for glass/epoxy in both temperatures. For the carbon/epoxy, the experimental values were found to be slightly above the theoretical ones for room temperature ageing and higher angles (±30° and ± 45° respectively). At room temperature, both composites demonstrate similar water uptake, while the carbon/epoxy samples appear to be more prone to absorption at a higher temperature, reaching up to 3 %, which is almost double that of the glass/epoxy.

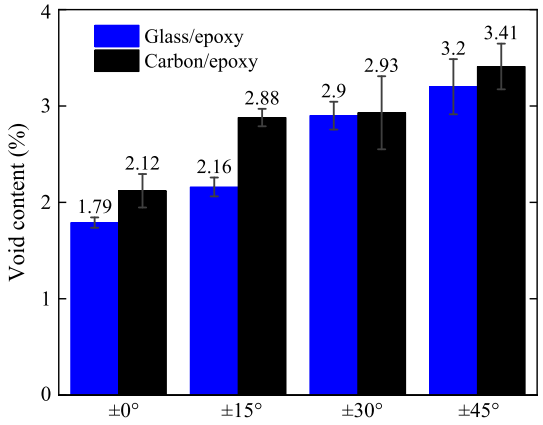

Fig. 3. Void content for non-aged glass/epoxy and carbon/epoxy composites.

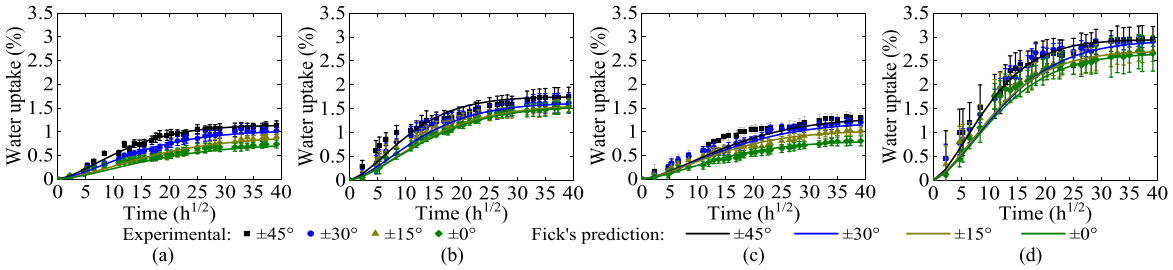

Fig. 4. Experimental results and theoretical predictions of water uptake for glass/epoxy at (a) 23 °C and at (b) 70 °C (b); and for carbon/epoxy at (c) 23 °C and at (d) 70 °C.

3.2. Fracture toughness of CDCB samples

The load–displacement (l-d) curves of all samples are presented in Fig. 5, for glass/epoxy, and in Fig. 6 for carbon/epoxy. The curves are organised based on fibre angle (columns) and type of ageing (rows). For the glass/epoxy samples (Fig. 5), the following considerations can be made:

- The composites wound at 0° have the lowest variation among all families. The structures wound at ± 15° and ± 45° have lower variation at the linear portion of the curves. The ± 30° samples have the highest variation in the elastic portion of the curve, attributed to an unfavourable fibre arrangement for this angle. The composites wound at ± 0° have brittle behaviour, and the others show a more ductile behaviour;
- The l-d curves suggest that the higher the fibre angle, the less stable is the crack propagation. The crack growth is very stable for the ± 0° samples, regardless of the ageing. Very unstable crack propagation is observed for the ± 30° samples, again due to the variation in stiffness, and the unfavourable helicoidal winding angle that prevents the crack from growing smoothly. The higher the fibre angle, the higher the peak load, since the fracture energy is highly dependent on the alignment of the fibres with the applied load;
- The different types of ageing do not significantly affect the shape of the curves. In general, hygrothermal ageing at room temperature does not significantly affect the peak load and shape of the curves. However, the ageing at 70 °C affects the composites in such a way that the peak load decreases for all fibre angles. Despite that, crack propagation is more stable for all fibre angles, especially for the specimens wound at ± 30°, which are very unstable when non-aged or aged at room temperature; and
- In general, the ageing at 70 °C yields more stable crack propagation in all samples.

The same observations can be generally applied for the carbon/epoxy composites, but they have a less ductile behaviour, especially those wound at ± 0°, compared to glass/epoxy, regardless of the ageing, and the peak loads are slightly higher. Interestingly, crack propagation for the carbon fibre composites is also more stable after ageing in hot water.

The R-curves (energy release rate *vs.* crack length extension) of all glass/epoxy samples are presented in Fig. 7, and those of carbon/epoxy are presented in Fig. 8. For the glass/epoxy composites the following observations can be made:

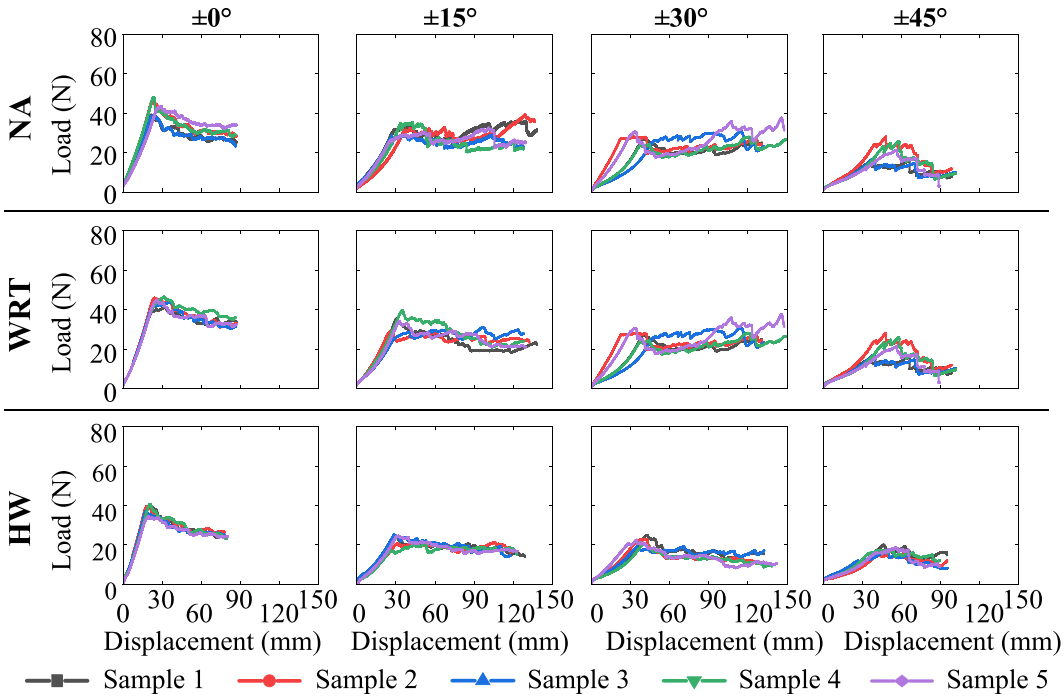

Fig. 5. Load-displacement curves for glass/epoxy composites under Mode-I fracture toughness (NA: non-aged, WRT: aged in water at room temperature; HW: aged in hot water).

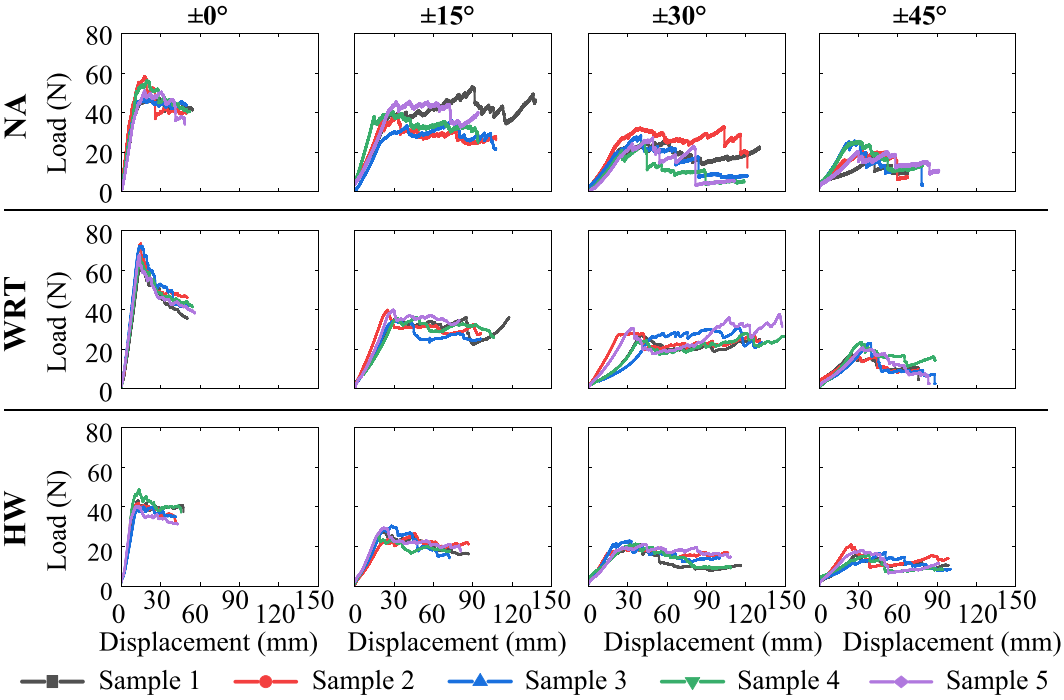

Fig. 6. Load-displacement curves for carbon/epoxy composites under Mode-I fracture toughness (NA: non-aged, WRT: aged in water at room temperature; HW: aged in hot water).

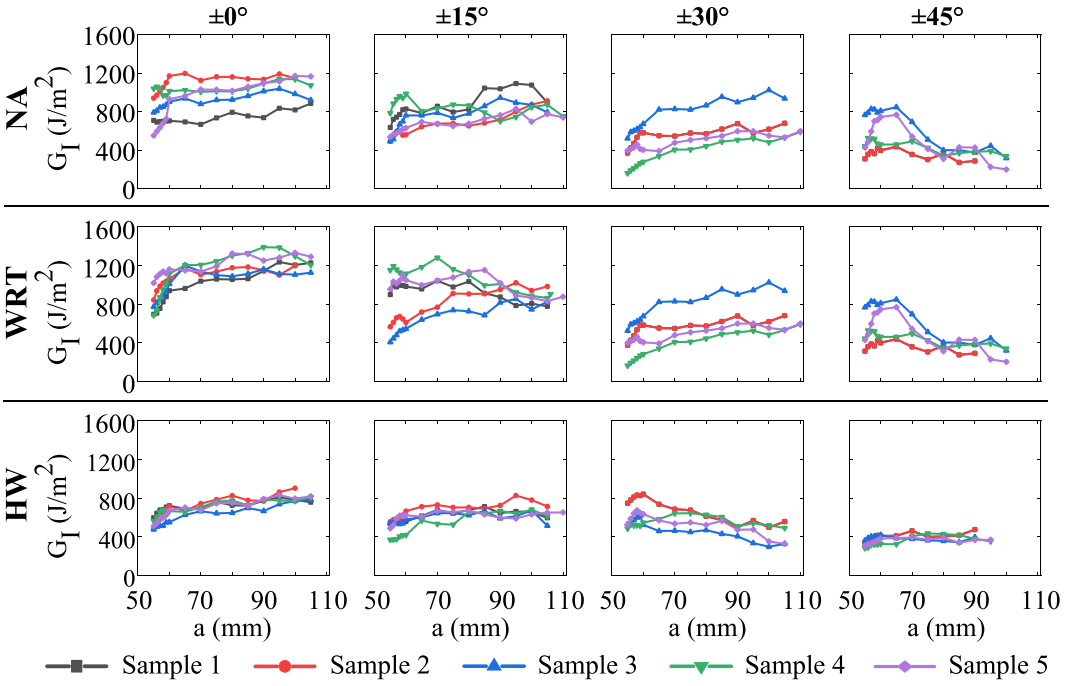

Fig. 7. The R-curves for all studied glass/epoxy composites.

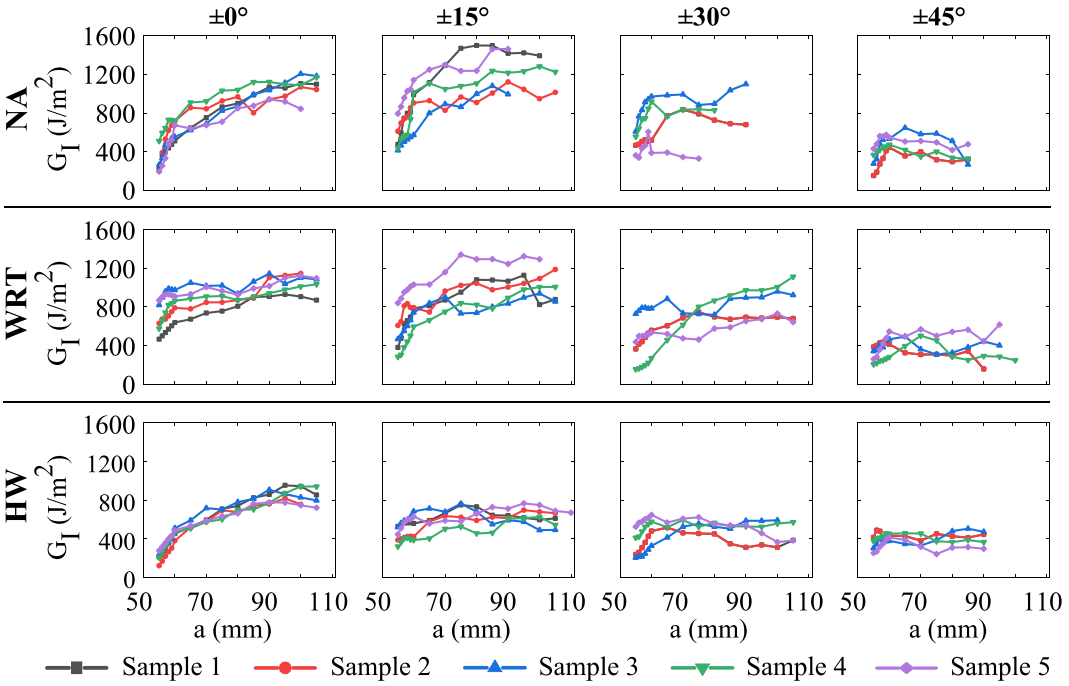

Fig. 8. The R-curves for all studied carbon/epoxy composites.

- Since the R-curves are strongly related to the load–displacement curves, the samples wound at ± 0° show the lowest variation in fracture toughness along the crack extension, i.e., the resistance to crack opening is more constant;
- The specimens wound at ± 15° show, in general, flat R-curves, but with higher variability than those wound at ± 0°;
- The samples wound at ± 30° non-aged and aged at room temperature present rising R-curves, and the samples wound at ± 45° are the only ones showing falling R-curves;

- As expected from the l-d curves, the R-curves indicate a more stable crack propagation for all fibre angles after ageing. And a more steady-state crack propagation is observed for those aged in hot water;
- Ageing at room temperature does not significantly affect energy release rate, but it heavily drops for the samples subjected to hot water ageing; and
- The shape of the R-curves does not change comparing non-aged and aged at room temperature composites. The non-aged and aged at room temperature samples wound at ± 0°, ±15° and ± 30° have rising R-curves. The R-curves for samples wound at ± 0° and ± 15° become flat when aged in hot water, whereas that for ± 30° goes from raising to falling. In addition, the shape of the R-curve for the specimens at ± 45° changes from falling to flat when going from non-aged to aged at room temperature and in hot water, which is very indicative of a material plasticisation phenomenon. Both the non-aged and the room-temperature aged samples demonstrate a fragile fracture behaviour with lower G_I values of crack propagation while the hot water-aged ones demonstrate more plastic behaviour, requiring more energy for crack propagation compared to initiation.

Fig. 8 presents the R-curves for the carbon/epoxy composites. Overall, the variation in G_I over the crack length is higher than those or the glass/epoxy composites. Besides:

- The variation in G_I along the crack length is the lowest for the samples wound at ± 0°, as expected. However, the samples at ± 15° show the highest variation, which decreases with increasing the fibre angle;
- The samples wound at ± 0° have stable crack growth in all cases, which does not occur especially for the ± 15° and ± 30° samples. Nonetheless, crack propagation is quite stable for all samples after ageing in hot water;
- The G_I values over the crack length decrease with increasing fibre angle, as expected, but these values are similar for samples wound at ± 0° and ± 15°. Then, they decrease for the other two fibre angles. This occurs regardless of the ageing;
- The samples wound at ± 0° have rising R-curves regardless of the ageing, the samples wound at ± 15° and ± 30° have rising R-curves for non-aged and aged at room temperature and flat R-curves for aged in hot water, whilst all ± 45° specimens have reasonably flat R-curves. Overall, the effect of the hot water ageing is evident for all winding angles, decreasing G_I for both crack initiation and propagation compared to the other samples, but with less variation between them; and
- The variation in G_I over the crack length decreases with the severity in ageing, similarly to glass/epoxy composites. Nevertheless, the decrease in G_I is lower for the samples aged in hot water compared to those non-aged or aged at room temperature.

4. Discussion

Based on the results presented, some comments could be made about the effectiveness of the curved samples in capturing the Mode-I fracture behaviour of filament-wound structures. In the case of CDCB specimens, the energy release values related to crack extension are higher than those related to the initiation, which indicates a not purely Mode-I crack opening, especially for samples with hoop (±0°) or low winding angles. In fact, considering that the composite structure is composed of interlaced tows, the micro-structure itself leads to the fibre bridging phenomenon, that is, fibre bundles connect the upper and lower parts of the fractured specimen, with a direct effect on the outcome of the test, as observed in past works [30–32].

To characterise fracture behaviour and crack propagation, representative images are taken during testing, shown in Fig. 9 for non-aged, Fig. 10 for aged at room temperature, and Fig. 11 for aged in hot water samples. Fibre bridging is observed in almost all cases, strongly contributing to the increased values of load for a given crack length. Another important aspect is the crack evolution plane, which may be considered stable in the case of hoop wound samples. In the other cases, crack extension was found to be locally unstable, which also reflects in the l-d curves (Fig. 5 and Fig. 6). In addition, the higher energy release rate values for crack propagation may be attributed to the crack extending to adjacent layers, as seen in Fig. 10.

As reported in other works in the field [30,32], there can be several failure modes coexisting in a specimen subjected to Mode-I crack opening. The development of a secondary crack is among the most common mechanisms, as observed in Fig. 9, combined with crack deflection to adjacent layers. Since the energy dissipation becomes greater, it may increase the energy release rate values related to crack propagation. In addition, when a crack jumps from the midplane to an adjacent layer, the system loses its symmetry and the thickness differs in the sides of the specimen thus deflecting it in an unbalanced manner, and hence affecting purity of the Mode-I crack propagation, as observed in some cases in both l-d and R-curves (e.g., rising R-curves). This may be noticed for the ± 15°, ±30° and ± 45° samples in both Fig. 10 and Fig. 11. This phenomenon is commonly observed in flat samples, and magnified for curved samples. The quite high intrinsic curvature of the samples herein studied, add significant complexity to the test. These observations are interesting, especially because curved filament-wound samples are poorly explored in the literature.

Fig. 12 presents a compilation of the G_{IC} values for all composites, calculated at a crack length of 60 mm, corresponding to a crack extension of 5 mm. For the glass/epoxy composites:

- The G_{IC} does not decrease with the increase in fibre angle and shows different trends with ageing. For instance, for non-aged samples, the G_{IC} decreases from ± 0° to ± 15°, then increases for ± 30°, and decreases for ± 45°, which has the lowest G_{IC} value. This is attributed to the variation in the fracture plane of the samples, which leads to different fracture mechanisms. If all samples failed under pure Mode-I, the G_{IC} values should decrease with the increase in fibre angle due to the higher offset in relation to the direction of the applied load; and
- The decrease in G_{IC} values as an effect of ageing at room temperature is evident for ± 30° and ± 45°. Another general observation is that the closer the fibre angle to hoop orientation, the lower the impact of this milder ageing. On the contrary, when samples are

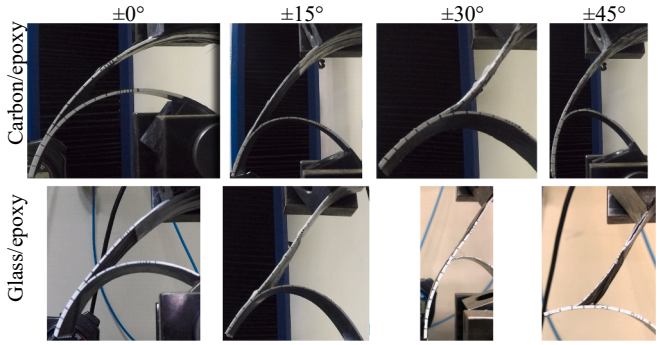

Fig. 9. Images of CDCB testing of non-aged samples.

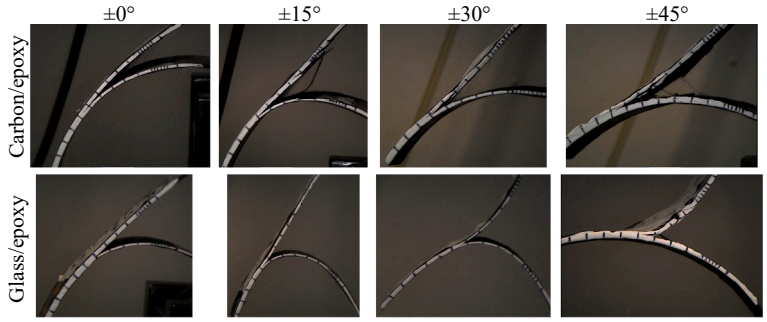

Fig. 10. Images of CDCB testing of samples aged in water at room temperature.

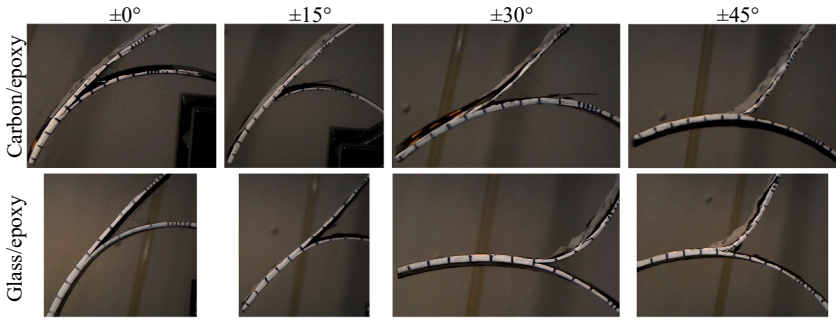

Fig. 11. Images of CDCB testing of samples aged in water at 70 °C.

subjected to ageing at 70 °C, the decrease in critical energy release values is far more significant. It should also be noted the higher standard deviation for the non-aged and room-temperature aged samples.

For the carbon/epoxy composites, the following considerations can be made:

- The average values of critical energy release rate are slightly lower compared to glass/epoxy composites, especially for aged hoop samples;
- Here again, the G_{IC} values are not decreasing for higher winding angle. Instead, there is a slight increase from ± 0° to ± 15°, followed by a decrease, along with a high standard deviation; and
- The WRT samples aged at room temperature show higher values compared to NA ones for hoop specimens. While NA samples display the highest G_{IC} values when wound at ± 15°, the WRT samples have similar critical energy levels. A similar trend is also seen for the HW samples. Nonetheless, the higher temperature aged samples show lower overall G_{IC} values.

The failure mechanisms reported in this experimental work can be found in larger structures under loads that open cracks in laminated composites following the Mode-I characteristic, i.e., crack opening or tensile forces acting perpendicular to the plane of the

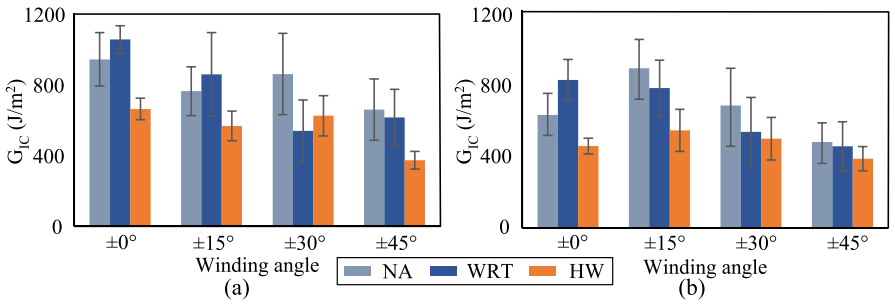

Fig. 12. Compilation of the average critical energy release rate for the (a) glass/epoxy and (b) carbon/epoxy curved composites.

crack. The parameters determined and discussed here are essential for designing composite structures that can withstand loading conditions and avoid catastrophic failure in applications ranging from aerospace components to civil engineering structures. Examples can be found in Zimmermann and Wang [32], who reviewed failure modes in aircraft composite structures, Grbović et al. [33] who evaluated the fracture characteristics of composite materials in aircraft engines, Savage et al. [34] who analyzed fracture of carbon fibre composites for energy absorbing structures, and also in Alderliesten [35], who reviewed usual approaches to assess fatigue and fracture in composite structures. Antunes et al. [36] analysed curing and seawater ageing effects on the mechanical behaviour of glass/epoxy filament wound cylinders under tension and compression.

5. Conclusion

This paper proposed a methodology to assess Mode-I fracture toughness of composite cylinders using curved double cantilever beam (CDCB) samples. Due to the lack of a dedicated standard, the experimental procedure was based on the established standard for Mode-I crack opening of flat composite samples. Glass/epoxy and carbon/epoxy filament-wound composites were evaluated. A further novelty involves experimentally determining the effect of ageing in room temperature or hot water on fracture toughness and critical energy release rate of these curved composites. This may aid the development of computational models that use these properties as input.

Comparably, the curved samples are more prone to show a combination of failure modes, such as parallel crack opening, crack progressing to adjacent layers and intense fibre bridging. Due to that, higher energy dissipation values for crack propagation were obtained, especially for non-hoop fibre-oriented specimens. Despite the challenging experimental test setup, the CDCB sample is effective in capturing fracture toughness and crack opening while the sample is subjected to Mode-I crack opening if the conditions allow the fracture to follow a controlled path.

The following conclusions can be drawn:

- The G_{IC} values of glass/epoxy non-aged (NA) samples follow a different trend compared to carbon/epoxy ones when the winding angle increases. For carbon/epoxy, the increase in the angle from ± 0° to ± 15° increases critical energy release rate, followed by a decrease for higher angle (±30°), with a G_{IC} similar to hoop-oriented samples;
- Less fibre bridging was observed for hygrothermally aged samples, especially those aged at a higher temperature. For both, glass and carbon composites, water absorption is expected to affect the matrix, leading to lower energy release rate values during crack propagation;
- The water uptake is strongly related to the void content. For both carbon and glass samples, the lowest values of both critical and propagation energy release rates were obtained for the samples wound at ± 45°. The combination of winding angle and void content of these samples magnifies the detrimental effects of ageing in harsh environments;
- Hoop-wound composite samples subjected to room temperature ageing have higher critical energy release rate values compared to the other angles Based on the more stable crack opening, the ± 0° samples are less affected by moisture, showing also slightly higher G_{IC} values compared to ± 30° and ± 45° samples. In general, the higher the winding angle, the more intense the effect of hygrothermal ageing at room temperature; and
- For both materials, the decrease in fracture toughness is more intense when aged in hot water. The high temperature enhances all fracture mechanisms related to the degradation of the matrix, the fibre/matrix interface and the interlaminar region, substantially decreasing fracture toughness as well as the critical and propagated energy release rate values.

A limitation in this study pertains to the impossibility of manufacturing cylinders at angles lower than ± 45°, thus preventing determining the toughness characteristics for samples with fibre angles between ± 45°- ±90°. Another limitation is regarding the unstable crack propagation for some samples attributed to the complex sample geometry.

CRediT authorship contribution statement

Artur Pollet: Formal analysis, Investigation, Methodology. **José Humberto S Almeida:** Conceptualization, Investigation,

Supervision, Validation, Visualization, Writing – original draft, Data curation, Formal analysis. **Antonios Stamopoulos:** Investigation, Visualization, Writing – original draft. **Sandro C. Amico:** Funding acquisition, Resources, Supervision, Writing – review & editing.

Declaration of competing interest

The authors declare that they have no known competing financial interests or personal relationships that could have appeared to influence the work reported in this paper.

Data availability

Data will be made available on request.

Acknowledgements

HA is supported by the Royal Academy of Engineering under the Research Fellowship scheme [Grant No. RF/201920/19/150]. AS acknowledges Green ComPASS project (Progetto di Avvio alla Ricerca). The authors also acknowledge the funding from FAPESP-FAPERGS (2019/15179-2 and 19/2551), CAPES/DAAD (PROBRAL 88881.198774/2018-01 and 57447163) and CNPq/EQUINOR (project No. 440115/2019-1).

References

[1] S.G.P. Castro, J.H.S. Almeida Jr, L. St-Pierre, Z. Wang, Measuring geometric imperfections of variable–angle filament–wound cylinders with a simple digital image correlation setup, Compos. Struct. 276 (2021) 114497, https://doi.org/10.1016/j.compstruct.2021.114497.
[2] A. Stamopoulos, L. Chiominto, E. Natale, A. Di Ilio, G. D'Emilia, Identification of the characteristics of helicoidally filament wound tubes using vision systems, Procedia Comput. Sci. 217 (2023) 1048–1056, https://doi.org/10.1016/j.procs.2022.12.303.
[3] C.B. Azevedo, J.H.S. Almeida Jr, H.F. Flores, F. Eggers, S.C. Amico, Influence of mosaic pattern on hygrothermally-aged filament wound composite cylinders under axial compression, J. Compos. Mater. 54 (19) (2020) 2651–2659, https://doi.org/10.1177/0021998319899144.
[4] J.H.S. Almeida Jr, H. Faria, A.T. Marques, S.C. Amico, Load sharing ability of the liner in type III composite pressure vessels under internal pressure, J. Reinf. Plast. Compos. 33 (24) (2016) 2274-2286, doi:10.1177/0731684414560221.
[5] Q. Wang, T. Li, B. Wang, C. Liu, Q. Huang, M. Ren, Prediction of void growth and fiber volume fraction based on filament winding process mechanics, Compos. Struct. 246 (2020) 112432, https://doi.org/10.1016/j.compstruct.2020.112432.
[6] E.A.W. Menezes, T.V. Lisbôa, J.H.S. Almeida Jr, A. Spickenheuer, S.C. Amico, R.J. Marczak, On the winding pattern influence for filament wound cylinders under axial compression, torsion, and internal pressure loads, Thin-Walled Struct. 191 (2023) 111041, https://doi.org/10.1016/j.tws.2023.111041.
[7] T.V. Lisbôa, J.H.S. Almeida Jr, A. Spickenheuer, M. Stommel, S.C. Amico, Marczak R.J FEM updating for damage modeling of composite cylinders under radial compression considering the winding pattern, Thin-Walled Struct. 173 (2022) 108954, https://doi.org/10.1016/j.tws.2022.108954.
[8] Y. Chang, Y. Zhou, N. Wang, K. Lu, W. Wen, Y. Xu, Micromechanical damage simulation of filament-wound composite with various winding angle under multi-axial loading, Compos. Struct. 313 (2023) 116925, https://doi.org/10.1016/j.compstruct.2023.116925.
[9] M.S. Uddin, E.V. Morozov, K. Shankar, The effect of filament winding mosaic pattern on the stress state of filament wound composite flywheel disk, Compos. Struct. 107 (2014) 260–275, https://doi.org/10.1016/j.compstruct.2013.07.004.
[10] J.H.S. Almeida Jr, L. St-Pierre, Z. Wang, M.L. Ribeiro, V. Tita, S.C. Amico, S.G.P. Castro, Design, modeling, optimization, manufacturing and testing of variable-angle filament-wound cylinders, Compos. B 225 (2021) 109224, https://doi.org/10.1016/j.compositesb.2021.109224.
[11] W. Toh, T.L. Bin, K.M. Tse, A. Giam, K. Raju, H.P. Lee, V.B.C. Tan, Material characterization of filament-wound composite pipes, Compos. Struct. 206 (2018) 474–483, https://doi.org/10.1016/j.compstruct.2018.08.049.
[12] R.F. Foral, Delamination failures in curved composite laminates, Key Eng. Mater. 37 (1989) 137–148, https://doi.org/10.4028/www.scientific.net/KEM.37.137.
[13] B. Lauke, K. Friedrich, Evaluation of processing parameters of thermoplastic composites fabricated by filament winding, Compos. Manuf. 4 (2) (1993) 93–101, https://doi.org/10.1016/0956-7143(93)90076-K.
[14] F. Ozdil, L.A. Carlsson, Characterization of mode-I delamination growth in glass/epoxy composite cylinders, J. Compos. Mater. 34 (5) (2020) 398–419, https://doi.org/10.1177/002199830003400503.
[15] G. Perillo, A.T. Echtermeyer, Mode-I fracture toughness testing of composite pipes, Appl. Compos. Mater. 20 (2013) 1135–1146, https://doi.org/10.1007/s10443-013-9318-7.
[16] Perillo G. and Echtermeyer A.T. Evaluation of Mode-I interlaminar fracture toughness of filament wound GFRE composite pipe. Proceedings of the 15th European Conference on Composite Materials ECCM15, 24-28 June 2012, Venice, Italy. ISBN: 978-88-88785-33-2.
[17] M.F. Abd Rased, S.H. Yoon, Experimental study on effects of asymmetrical stacking sequence on carbon fiber/epoxy filament wound specimens in DCB, ENF, and MMB tests, Compos. Struct. 264 (2021) 113749, https://doi.org/10.1016/j.compstruct.2021.113749.
[18] Taylor J.M., Frenz S., Canturri C., Giannis S., Greenhalgh E.S. Mode-I and Mode-II fracture behaviour of carbon/glass hybrid filament-wound resin transfer moulded composites. Proceedings of the 16th European Conference on Composite Materials ECCM16, 22-26 June 2014, Seville, Spain.
[19] B.C. Ray, Temperature effect during humid ageing on interfaces between glass and carbon fibers reinforced epoxy composites, J. Colloid Interface Sci. 298 (1) (2006) 111–117, https://doi.org/10.1016/j.jcis.2005.12.023.
[20] P. Krishnan, M.S. Abdul Majid, M. Afendi, S. Yaacob, A.G. Gibson, Effects of hydrothermal ageing on the behaviour of composite tubes under multiaxial stress ratios, Compos. Struct. 148 (2016) 1–11, https://doi.org/10.1016/j.compstruct.2016.03.055.
[21] S.N. Fitriah, M.S. Abdul Majid, M.J.M. Ridzuan, R. Daud, A.G. Gibson, T.H. Assaleh, Influence of hydrothermal ageing on the compressive behaviour of glass fibre/epoxy composite pipes, Compos. Struct. 159 (2017) 350–360, https://doi.org/10.1016/j.compstruct.2016.09.078.
[22] A. Hawa, M.S. Abdul Majid, M. Afendi, H.F.A. Marzuki, N.A.M. Amin, F. Mat, A.G. Gibson, Burst strength and impact behaviour of hydrothermally aged glass fibre/epoxy composite pipes, Mater. Des. 89 (2016) 455–464, https://doi.org/10.1016/j.matdes.2015.09.082.
[23] E. Vargas-Rojas, Prescriptive comprehensive approach for the engineering of products made with composites centered on the manufacturing process and structured design methods: review study performed on filament winding, Compos. B 243 (2022) 110093, https://doi.org/10.1016/j.compositesb.2022.110093.
[24] I.S. Floros, K.I. Tserpes, T. Löbel, Mode-I, mode-II and mixed-mode-I+II fracture behaviour of composite bonded joints: experimental characterization and numerical simulation, Compos. B 78 (2015) 459–468, https://doi.org/10.1016/j.compositesb.2015.04.006.
[25] A.G. Stamopoulos, S.I. Scipioni, F. Lambiase, Experimental characterization of the interlayer fracture toughness of FDM components, Compos. Struct. 320 (2023) 117213, https://doi.org/10.1016/j.compstruct.2023.117213.
[26] J.H.S. Almeida Jr, S.D.B. Souza, E.C. Botelho, S.C. Amico, Carbon fiber-reinforced epoxy filament-wound composite laminates exposed to hygrothermal conditioning, J. Mater. Sci. 51 (2014) 4697–4708, https://doi.org/10.1016/S0034-3617(06)70913-4.

[27] F. Eggers, J.H.S. Almeida Jr, T.V. Lisbôa, S.C. Amico, Creep and residual properties of filament-wound composite rings under radial compression in harsh environments, Polymers. 13 (2021) 33, https://doi.org/10.3390/polym13010033.
[28] A. Sidique, S. Abid, F. Shafiq, Y. Nawab, H. Wang, B. Shi, S. Saleemi, B. Sun, Mode-I fracture toughness of fiber-reinforced polymer composites: a review, J. Ind. Text. 50 (8) (2021) 1165–1192, https://doi.org/10.1177/1528083719858767.
[29] A.G. Stamopoulos, A.P. Psaropoulos, K. Tserpes, Experimental and numerical investigation of the effects of porosity on the in-plane shear properties of CFRPs using the V-notched rail shear test method, Int. J. Mater. Form. 14 (2021) 67–82, https://doi.org/10.1007/s12289-020-01544-1.
[30] N. Nasuha, A.I. Azmi, C.L. Tan, A review on mode-I interlaminar fracture toughness of fibre reinforced composites, J. Phys. Conf. Ser. 908 (2017) 012024, https://doi.org/10.1088/1742-6596/908/1/012024.
[31] N. Zimmermann, P.H. Wang, A review of failure modes and fracture analysis of aircraft composite materials, Eng. Fail. Anal. 115 (2020) 104692, https://doi.org/10.1016/j.engfailanal.2020.104692.
[32] A. Grbović, G. Kastratović, Ž. Božić, I. Božić, A. Obradović, A. Sedmak, S. Sedmak, Experimental and numerical evaluation of fracture characteristics of composite material used in the aircraft engine cover manufacturing, Eng. Fail. Anal. 137 (2022) 106286, https://doi.org/10.1016/j.engfailanal.2022.106286.
[33] G. Savage, I. Bomphray, M. Oxley, Exploiting the fracture properties of carbon fibre composites to design lightweight energy absorbing structures, Eng. Fail. Anal. 11 (5) (2004) 677–694, https://doi.org/10.1016/j.engfailanal.2004.01.001.
[34] R. Alderliesten, Critical review on the assessment of fatigue and fracture in composite materials and structures, Eng. Fail. Anal. 35 (2013) 370–379, https://doi.org/10.1016/j.engfailanal.2013.03.022.
[35] M.B. Antunes, J.H.S. Almeida Jr, S.C. Amico, Curing and seawater aging effects on mechanical and physical properties of glass/epoxy filament wound cylinders, Compos. Commun. 22 (2020) 100517, https://doi.org/10.1016/j.coco.2020.100517.